Research Article | Vol. 14, No. 6 / 1 Jun 2023 / Biomedical Optics Express 3086
Biomedical Optics EXPRESS

Adaptive window space direction laser speckle contrast imaging to improve vascular visualization

GUANG HAN,[1,2] DE LI,[1] JIWEI WANG,[3] QIANBEI GUO,[4] JIXIN YUAN,[1] RUIJUAN CHEN,[1,2] JINHAI WANG,[1,2] HUIQUAN WANG,[1,2] AND JUN ZHANG[1,2,*]

[1]School of life Sciences, Tiangong University, Tianjin, 300387, China
[2]Tianjin Key Laboratory of Quality Control and Evaluation Technology for Medical Devices, Tianjin 300387, China
[3]Departments of Neurosurgery, Tianjin Huanhu Hospital, Tianjin Key Laboratory of Cerebral Vascular and Neurodegenerative Diseases, Tianjin, 300350, China
[4]School of Electrical and Electronic Engineering, Tiangong University, Tianjin 300387, China
*zhang6216937@163.com

Abstract: Vascular visualization is crucial in monitoring, diagnosing, and treating vascular diseases. Laser speckle contrast imaging (LSCI) is widely used for imaging blood flow in shallow or exposed vessels. However, traditional contrast computation using a fixed-sized sliding window introduces noise. In this paper, we propose dividing the laser speckle contrast image into regions and using the variance criterion to extract pixels more suitable for the corresponding regions for calculation, and changing the shape and size of the analysis window at the vascular boundary regions. Our results show that this method has a higher noise reduction and better image quality in deeper vessel imaging, revealing more microvascular structure information.

1. Introduction

The microvasculature is a crucial component of the human body that enables the delivery of vital nutrients to support the normal functioning of life. However, disruptions in the microvascular system have been linked to the development of various chronic diseases and vascular diseases [1]. For example, diabetes is a common chronic disease in which hyperglycemia leads to dysfunction of the microvasculature. The functional response of microvasculature has been studied as a potential marker for early warning of diabetes [2,3]. In addition, ocular microvascular visualization can be used as an alternative to intracerebral angiography to study the pathological process of cerebral small vessels disease and vascular cognitive impairment (VCI) [4]. Therefore, the monitoring of morphological changes and alterations in the microvasculature is a critical aspect of understanding the progression of diseases and evaluating therapeutic interventions. In conclusion, the visualization of microvessels holds immense significance in the medical field, as it can provide crucial insights into the mechanisms of early vascular disease, thereby leading to the formulation of effective treatment strategies.

Laser speckle contrast imaging (LSCI) has become a widely used optical imaging technique for the visualization of blood vessels and dynamic monitoring of blood flow, owing to its non-invasiveness, lack of requirement for a contrast agent, ease of use without scanning, and high spatial and temporal resolution [5]. Specifically, LSCI has the ability to generate retinal flow maps in a cost-effective and noninvasive manner, which can aid in identifying various ocular conditions linked to reduced blood flow [6]. Moreover, LSCI offers a scalable field of view, as the imaging system can be adjusted with minimal changes to facilitate either high-resolution blood flow imaging through cranial windows or low-resolution perfusion visualization of perfusion

#488054 https://doi.org/10.1364/BOE.488054
Journal © 2023 Received 21 Feb 2023; revised 6 May 2023; accepted 22 May 2023; published 1 Jun 2023

Biomedical Optics EXPRESS

across larger areas, such as in human skin. This versatility allows LSCI to be utilized for investigating vasoreactivity in renal microcirculation by monitoring global blood flow changes across the renal surface [7]. The principle of LSCI involves the irradiation of the surface of biological tissue with laser light, and the subsequent interaction of the coherent light with the scattering particles in the tissue. By quantifying the fluctuations in light intensity caused by the movement of these scattering particles, the imaging of vascular structures and blood flow velocity within the tissue becomes possible. At the same time, when the laser light is backscattered from the tissue, it produces a time-dependent speckle pattern, and the measurement of the speckle decorrelation time can provide information about the tissue dynamics [8]. Currently, common LSCI methods such as spatial contrast (sK), temporal contrast (tK), and spatial-temporal contrast (stK) have enabled visualization of superficial vessels [9]. However, when it comes to deep vascular imaging ($>300\mu m$), the high noise level of the contrast image (CI) formed from dispersed photons scattered by perivascular tissue leads to a significant reduction in image quality and visual representation of blood vessels [10]. However, compared with the spatial domain method, the tK is less affected by static speckle. In the presence of substantial static optical scattering, the tK also has the potential to accurately assess blood flow changes within a single exposure time [11]. In digital images of biological tissues, speckles formed from tissue scattering are referred to as static speckles and do not contain any useful information. The high dispersion in gray values, also known as noise [12], further exacerbates the situation.

Numerous studies have aimed to improve the calculation of contrast in order to mitigate the noise present in LSCI. One such approach, the anisotropic contrast (aK) method [13], seeks to calculate the local blood vessel contrast along the estimated blood flow direction with the smallest contrast gradient by determining the contrast gradients of each direction in the analysis window based on the center pixel. This method demonstrates a reduction in noise in the vessel area by only considering pixels in the direction of blood flow when calculating the contrast of the vessel position, and also maintains a high temporal resolution through the use of only three frames of speckle images. Another approach, the Space-directional contrast (sdK) method [14,15], takes into account the dynamic changes of each frame, calculating the pixel variance corresponding to each direction in each analysis window and selecting the maximum direction as the available pixel for contrast calculation. This method demonstrates a reduction in noise. The Adaptive window contrast (awK) method [16], which calculates the contrast by selecting pixels in the same area as the center pixel in the sliding window through region partitioning of the image, has been proposed to improve the visualization effect of the blood vessel edge.

In this study, we present a novel method to mitigate noise and enhance the imaging quality of deeper blood vessels while preserving high temporal resolution. The proposed approach leverages the independence of the original speckle image (OSI) by dividing each frame into independent regions. To minimize the introduction of noise, an adaptive window is employed at the boundary between dynamic and static regions for contrast calculation. The pixel orientation within the analysis window for each region is selected using a variance criterion to accurately calculate the contrast value representative of the region. Our results demonstrate that our method significantly improves the imaging quality of deep blood vessels compared to other existing methods. The method achieves higher contrast-to-noise ratio (CNR) and displays more detailed small vessel motion information, enhancing the capability of microvascular visualization.

2. Theory

2.1. Experimental setup

2.1.1. Skin phantom

In vitro phantom experiments, we used a skin model (Fig. 1(b)) to simulate the dermis and epidermis. The dermis was simulated with pure epoxy resin containing titanium dioxide

Biomedical Optics EXPRESS

(3.2 mg/ml) and India ink (1.6 mg/ml). The epidermis was simulated with pure epoxy resin containing titanium dioxide (5.5 mg/ml) and India ink (2.5 mg/ml). The concentration of TiO_2 was used to mimic the reduced scattering coefficients of dermis ($\mu_s = 2.3mm^{-1}$) and epidermis ($\mu_s = 3.7mm^{-1}$), respectively. India ink is used to mimic melanin in the skin, where the concentration is used to mimic the absorption coefficient characteristics of the dermis ($\mu_a = 0.12mm^{-1}$) and epidermis ($\mu_a = 0.18mm^{-1}$), respectively [17]. Capillary glass tubes (inner diameter = 1 mm, outer diameter = 2 mm) were used to mimic straight vessels, which were embedded horizontally and level with the top of the dermis. Epidermal layers of varying thickness ($0 \sim 500\mu$m) were placed on top of the dermis to mimic vascular depth. The depth measurements as well as the preparation of the epoxy samples were performed as follows: Make horizontal holes on both sides of the silicone mold and insert the capillary glass tube. First, the epoxy resin dermal solution was prepared and added into the silicone mold to the top of the capillary glass tube. After solidification, it was first polished with coarse sandpaper, and the vernier caliper was used to measure the distance. When the distance between the surface layer and the top of the glass tube was close to 0μm, then polished with fine sandpaper to 0μm. When a sample with a depth of 200μm was required, an epoxy resin epidermis solution was configured, added to the sample with a depth of 0μm, and after solidification, it was ground to 200μm using the same method.

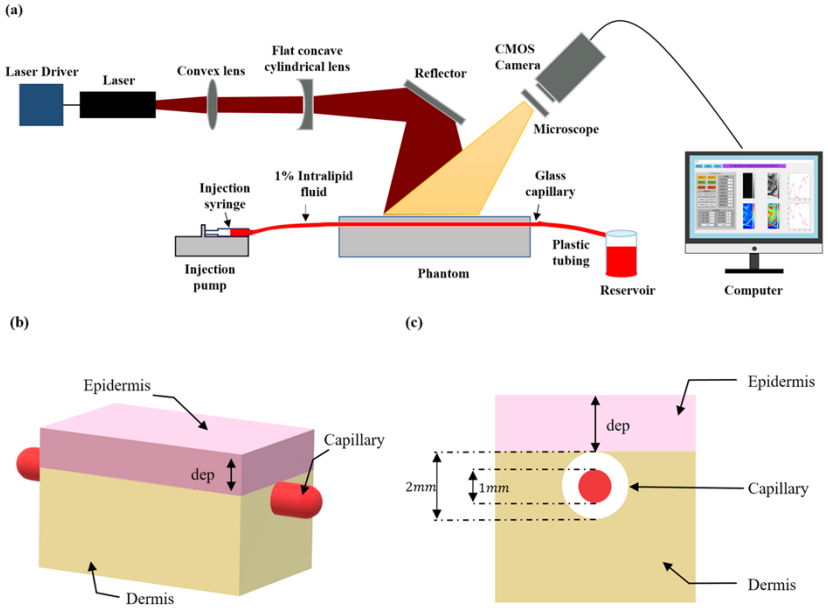

Fig. 1. a) Experimental setup for the acquisition of OSIs in vitro. b) Skin models used to simulate blood vessel at different depths. Three layers were simulated: epidermis, capillaries, and dermis. c) Schematic cross-section of the skin model.

2.1.2. Laser speckle contrast imaging setup

Figure 1(a) shows the experimental setup used to acquire the laser speckle image. The light source consists of a DBR single-frequency laser diode (λ = 785nm, PH785DBR, Photodigm) and a laser diode controller (W = 40mW, LDC-3908 model, ILXlightwava). The emitted laser light was focused by a convex lens (LB1630-B, Thorlabs), expanded by a flat concave cylindrical lens (GL16, Golden Way Scientific, China), and reflected by a mirror (ME2S-M01, Thorlabs) to uniformly illuminate the skin model. The backscattered light from the sample was captured by a

Biomedical Optics EXPRESS

sCMOS camera (Zyla-4.2, Andor) equipped with a microscope lens (S Fluor, 4x/0.20, WD = 15.5, Nikon). The sCMOS camera exposure time was 5 ms. A 1% fat emulsion solution was used to mimic blood, and the flow rate of the liquid in the capillary glass tube was controlled by means of a syringe and syringe pump (SPM, DK INFUSETEK, China).

2.2. Contrast calculation

The OSI is a representation of the distribution of integrated light intensity that is formed through the random coherent superposition of scattered coherent light at a given exposure time. Movement within biological tissues can result in a fluctuation of light intensity and result in a blurrier speckle pattern. Within these tissues, the OSI can be divided into two distinct regions: a static region, typically corresponding to skin tissue, and a dynamic region, which corresponds to blood vessels. The blurriness of the speckle pattern in this dynamic region contains valuable information regarding blood flow motion [18]. The degree of blurring can be quantified using the contrast value, which is defined as the ratio of the standard deviation (σ) of light intensity to the mean value ($\langle I \rangle$) of light intensity. Contrast value is defined as follows:

$$K = \frac{\sigma}{\langle I \rangle} \tag{1}$$

The contrast values were between 0 and 1. If the contrast value is infinitely close to 1, it indicates that the region has no motion and is located in the static region. If the contrast value is infinitely close to 0, it indicates that the region moves quickly and is located in the dynamic region. The light intensity values between pixels in the dynamic region are more similar than those between pixels in the static region, so the standard deviation of light intensity in the dynamic region is lower and the contrast value is lower.

In the field of laser speckle contrast analysis, several methods have been developed for the generation of speckle contrast images. The sK method, as described in Ref. [19] (Fig. 2(a)), involves the selection of a fixed spatial sliding window of size N × N, where N commonly takes on values of 3, 5, or 7. The contrast within the sliding window is calculated according to Eq. (1) and is assigned to the central pixel (P) of the sliding window. The sliding window traverses the rows and columns of the entire speckle image to generate a spatial contrast image. However, it is commonly observed that a single spatial contrast image exhibits higher levels of noise. To address this issue, the average spatial contrast (asK) method, as described in Ref. [20] (Fig. 2(b)), was developed to mitigate the issue of high noise in a single spatial contrast image. This approach entails computing the average of multiple spatial contrast images to obtain a single average spatial contrast image, thereby yielding an improvement in noise reduction. However, it should be noted that this improvement comes at the cost of decreased temporal resolution. The tK method, described in Ref. [21] (Fig. 2(c)), selects a fixed time series window for each pixel in space for a series of temporally continuous speckle images. The temporal contrast value at each point is calculated according to Eq. (1), and this process is repeated for each pixel in space to generate the temporal contrast image. Although the tK method has higher spatial resolution compared to sK and asK, it sacrifices temporal resolution. Finally, the sdK method, described in Ref. [14] (Fig. 2(d)), considers the difference in light intensity fluctuation between the static and dynamic regions of the speckle image. Pixels in the 0°, 45°, 90°, and 135° directions within the sliding window are selected for calculation, and the direction exhibiting the largest variance is used to calculate the contrast value. This approach eliminates the reliance on a single calculation direction and accounts for dynamic variations between frames.

2.3. Anisotropic diffusion filter

The anisotropic diffusion filter (ADF) algorithm has demonstrated its effectiveness in smoothing images while retaining the edges, thereby preserving the vascular structure information in LSCI

Biomedical Optics EXPRESS

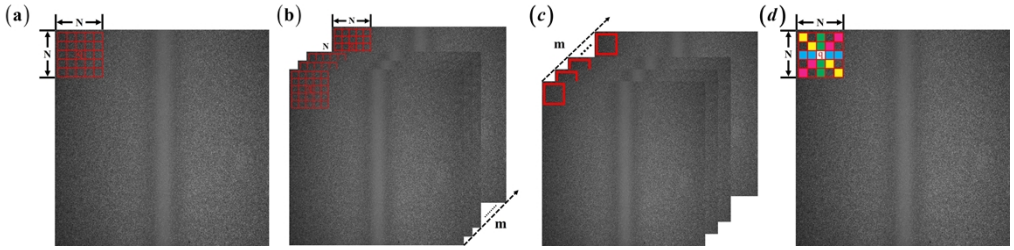

Fig. 2. Laser speckle contrast method. a) Spatial contrast method (sK). b) Average spatial contrast method (asK). c) Temporal contrast method (tk). d) Space-directional contrast method (sdK).

to a greater extent. In the filtering method [22], the entire image is regarded as a heat field, with each pixel treated as a heat flow. The diffusion of the current pixel to its surrounding pixels is determined based on the relationship between the current pixel and the surrounding pixels. A non-uniform process is employed to reduce the diffusion of edges. This smoothing process is not confined within homogeneous regions, while it is suppressed in cross-boundary regions, preserving the edge features of the image while smoothing the noise. The laser speckle contrast image was used as the raw input and iteratively calculated using Eq. (2) and Eq. (3) [23,24].

$$K(x,y)_{(n+1)} = K(x,y)_n + \lambda \times (d_N \cdot \nabla K_N + d_S \cdot \nabla K_S + d_E \cdot \nabla K_E + d_W \cdot \nabla K_W) \tag{2}$$

$$d(\nabla K) = \frac{1}{1 + \left(\frac{\nabla K}{K_t}\right)^2} \tag{3}$$

Where n is the number of filtering iterations. λ represents the rate of heat diffusion, and since the four directions are taken, namely north, south, east and west, λ is taken as 0.25. d is the diffusion coefficient. ∇K is the contrast gradient calculated according to the difference between the center pixel and the neighboring pixels in a specific direction. K_t is the edge magnitude parameter, which can be determined using the average contrast of the contrast image obtained in the previous iteration.

2.4. K-means clustering algorithm

The k-means clustering algorithm is a well-known and widely used clustering method that aims to measure the similarity of each data point in a dataset based on the minimum distance from each cluster center [25]. The algorithm divides the dataset into K classes, iteratively minimizing the distance of each data point to its class center, with each data point belonging to only one class. The resulting clustering minimizes the corresponding loss function [26] as defined in Eq. (4).

$$J = \sum_{i=1}^{K} \sum_{j=1}^{M} r_{ij} \cdot \left\| x_j - {\mu_{k_i}}^2 \right\| \tag{4}$$

$$r_{ij} = \begin{cases} 1, & if\ x_j \in k_i \\ 0, & else \end{cases} \tag{5}$$

Where M represents the total number of data points. x_j represents the value of the jth data point. K stands for the number of clusters. k_i represents the ith cluster. μ_{k_i} represents the center value corresponding to the ith cluster. The algorithm selects the initialized K samples as the initial cluster center, calculates the distance from each data point x_j to the K cluster center in the data set and divides it into the class corresponding to the cluster center with the minimum

Biomedical Optics EXPRESS

distance. For each class k_i, its cluster center is re-calculated until the loss function is the minimum. K-means clustering algorithm is characterized by a low computational complexity. The use of this algorithm for image segmentation yields good segmentation results, while incurring low computational costs and fast processing speeds, thus reducing the overall time complexity of the algorithm.

2.5. Contrast to noise ratio

The Contrast to noise ratio (CNR) is a metric that quantifies the image contrast [27] and is utilized in various Laser Speckle Contrast Imaging (LSCI) methods to assess image quality. It offers the information regarding the discrepancy between the contrast of static regions and dynamic regions of laser speckle images. The CNR is linked to the contrast differences between static and dynamic regions, as well as the visibility of blood vessels in the surrounding background tissue. The definition of CNR is as follows [13]:

$$\mathrm{CNR} = \frac{|\mu_{vessels} - \mu_{tissue}|}{\sigma_{tissue}} \tag{6}$$

Where $\mu_{vessels}$ and μ_{tissue} tissue are the average speckle contrast values of vessels and tissue regions, respectively, and σ_{tissue} is the standard deviation of the background tissue speckle contrast values. The higher the CNR, the greater the contrast difference between the vascular region and the surrounding tissue region. In terms of noise reduction, a higher CNR value is associated with improved visualization of vessels.

3. Adaptive window space direction contrast method

During the formation of the OSI, dynamic speckles generated by the movement of red blood cells within blood vessels and static speckles generated by the static tissues surrounding the blood vessels both exist and are superimposed on the image plane. With increasing imaging depth, the dynamic regions are increasingly impacted by the presence of static speckles, leading to a reduction in the visualization of blood vessels in these regions, particularly for microvessels that possess small diameters and slow flow speeds. The presence of noise within the analysis window may also obscure its own contrast changes, leading to a loss of vital vascular information. For the purposes of this study, high-intensity fluctuations caused by tissue scattering are considered to be noise. In OSI, the light intensity values in the dynamic regions exhibit a higher degree of similarity, whereas those in the static regions exhibit a high degree of dispersion. As a result, the calculated contrast values in the dynamic regions are more concentrated than those in the static regions (Fig. 4(a) and 4(b)). In the case of the LSCI method, both temporal resolution and noise reduction are critical considerations, however there are often trade-offs in the application of these methods. Furthermore, in OSI with high noise levels, the CI calculated by selecting the best direction or window size may still be impacted by noise. Thus, it is imperative to consider how to achieve significant noise reduction and obtain more vascular information while maintaining high temporal resolution for CI.

We propose the following considerations: (1) Determine the pixel region processed in the sliding analysis window, select the pixels that are most suitable for static or dynamic regions for calculation, and reduce the introduction of noise at the boundaries of vessels and tissues. (2) Measure based on variance as the standard, select fluctuations in light intensity to avoid the impact of outliers. The adaptive window space direction contrast (awsdK) algorithm is proposed based on the intensity fluctuation characteristics of dynamic and static regions. In this method, criterion-based pixel sets are selected for calculation in different analysis regions, and the contrast calculation direction is selected based on specific variance criteria. In the boundary region where the vessels and tissue are connected, the selection criterion for the pixel set is the similarity between the center pixel q in the sliding analysis window and the surrounding

Biomedical Optics EXPRESS

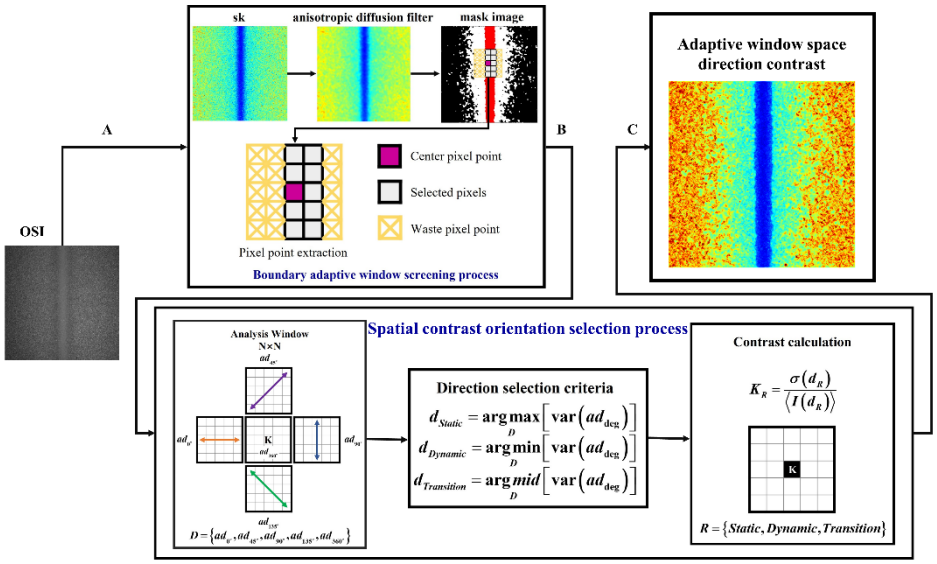

Fig. 3. The proposed adaptive window space direction contrast (awsdK) algorithm: (A) A mask was made for OSI, and the actual calculated pixels within the sliding window were screened; (B) The direction for calculating the contrast value was chosen based on the variance criterion; (C) The contrast value of OSI was recalculated to obtain the adaptive window space direction contrast image.

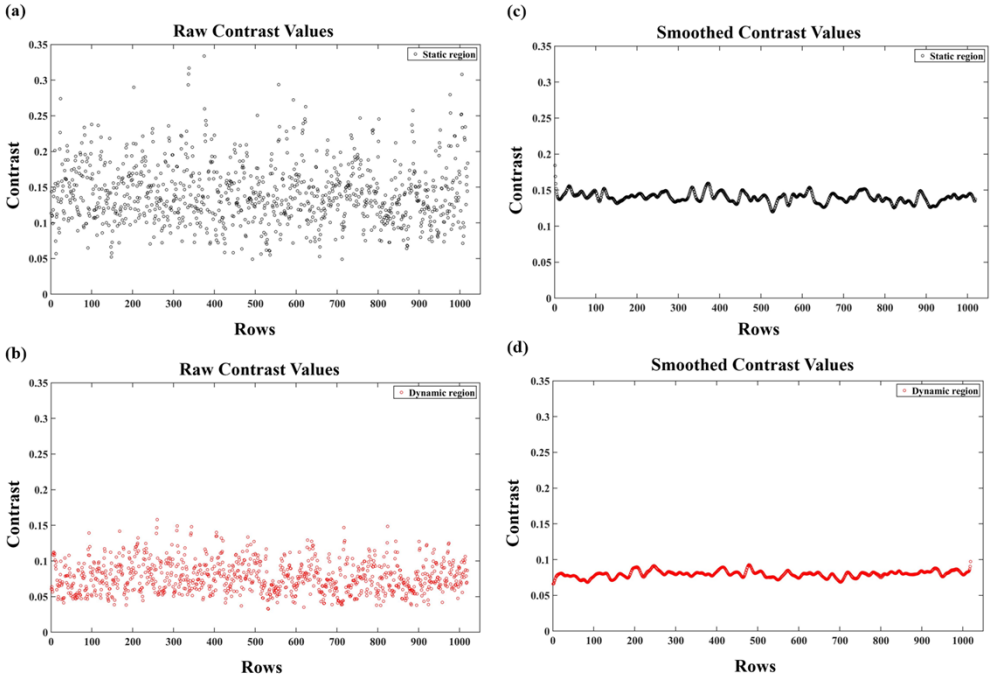

Fig. 4. Scatter plot of the representation of the dynamic and static regions. a) Scatter plot of static regions. b) Scatter plot of dynamic regions. c) Scatter plot of the static regions after ADF. d) Scatter plot of the dynamic regions after ADF.

Biomedical Optics EXPRESS

neighborhood pixels. The sliding analysis window can be adjusted based on the region where the center pixel q is located to achieve noise attenuation while maximizing the retention of relevant data. When there is no obvious difference between the pixels in the window, the variance is calculated in different directions and the global region in the window. Dynamic regions select pixels with the minimum variance, static regions select pixels with the maximum variance, and transitional regions between dynamics and statics select median variance pixels for contrast value calculations. The variance of dynamic regions is small and the similarity between pixel values is high. Selecting the minimum variance can better remove the impact of outliers of static scattered noise. In static regions, the maximum variance is selected for calculation, and the contrast value in static regions will increase compared to the contrast value calculated by the traditional method. Therefore, the contrast difference between static regions and dynamic regions will increase, and the visualization of dynamic regions will be improved. Figure 3 shows the contrast value calculation process of the awsdK method.

The mask image (MI) is used to calibrate the analysis regions, and it is obtained by segmenting the CI. However, the dispersion of dynamic and static regions in CI can lead to difficulties in obtaining an appropriate MI, particularly in LSCI. To reduce the influence of outliers on regional analysis, filters are recommended to be used to attenuate noise enhancement caused by increased tissue thickness. When filtering CI, it is important to maintain the original vascular structure as CI usually contains multi-diameter vascular plexus instead of just a single vessel. Common filters such as mean and median filters may cause loss of edge information while smoothing the image. However, using ADF is an edge-sensitive filter that can maintain image details while denoising and smoothing, and has the advantage of fast processing. After ADF filtering, the differentiation between regions in CI is enhanced. K-means clustering algorithm is then employed to segment the denoised CI into k clusters to obtain the MI, with different k values selected based on the classification effect of CI. For instance, when k = 2, MI contains static (black) and dynamic (red) clusters. When k = 3, MI includes static (black), dynamic (red), and dynamic-static transition states (white) clusters.

Then, according to MI, the sliding window was judged to be located in the region of OSI, and different calculation criteria were adopted for different regions to recalculate the contrast value. If the sliding window is located in the boundary region, the pixels within the sliding window with the same cluster as the central pixel of the sliding window are selected to recalculate the contrast value. The calculation formulas are as follows: Eq. (7) and Eq. (8).

$$K(x,y,z) = \frac{\sqrt{\frac{1}{C}\sum_{i=1}^{W}\sum_{j=1}^{W}\left(I_{W1}(i,j,z) - \overline{I_{W1}(z)}\right)^2}}{\overline{I_{W1}(z)}} \tag{7}$$

$$\overline{I_{W1}(z)} = \frac{1}{C}\sum_{i=1}^{W}\sum_{j=1}^{W} I_{W1}(i,j,z) \tag{8}$$

Where, $I_{W1}(i,j,z)$ is the pixel light intensity value belonging to the same cluster as the center pixel in the sliding window. C is the number of pixels involved in calculating the contrast value.

if the sliding window is not in the boundary region, the following criteria are used to calculate the contrast value. Firstly, all pixels ad_{360° in the sliding window and pixels ad_{0°, ad_{45°, ad_{90°, and ad_{135° in the four directions constitute d_n. As shown in Eq. (9) and Fig. 5. if the sliding window is located in the static region, the pixel in the direction with the largest variance within the sliding window is selected to calculate the contrast value. As shown in Eq. (10). if the sliding window is located in the dynamic and static transition region, the pixels in the direction of the median variance in the sliding window are selected to calculate the contrast value. As shown in Eq. (11). if the sliding window is located in the dynamic region, the pixel in the direction with the smallest variance within the sliding window is selected to calculate the contrast value. As shown in Eq. (12). The OSI contrast value was recalculated with the above criteria, and the

Biomedical Optics EXPRESS

results of awsdK method were obtained. The proposed method is applied to each OSI separately to ensure the independence between images, taking into account the dynamic changes between each frame. When the number of OSI frames is greater than 1, the obtained multi-frame awsdK image is averaged to achieve the purpose of further attenuating noise, and the single frame image is the final result without averaging.

$$d_n = \{ad_{0^\circ}, ad_{45^\circ}, ad_{90^\circ}, ad_{135^\circ}, ad_{360^\circ}\} \tag{9}$$

$$\begin{cases} d_{static} = \arg_d \max[var(d_n)] \\ K_{static}(x,y) = \frac{\sigma(d_{static})}{\overline{d_{static}}} \end{cases} \tag{10}$$

$$\begin{cases} d_{transition} = \arg_d \text{median}[var(d_n)] \\ K_{transition}(x,y) = \frac{\sigma(d_{transition})}{\overline{d_{transition}}} \end{cases} \tag{11}$$

$$\begin{cases} d_{dynamic} = \arg_d \min[var(d_n)] \\ K_{dynamic}(x,y) = \frac{\sigma(d_{dynamic})}{\overline{d_{dynamic}}} \end{cases} \tag{12}$$

Where, d_{static}, $d_{transition}$, and $d_{dynamic}$ represent the set of pixels in the direction of maximum variance, median variance, and minimum variance, respectively.

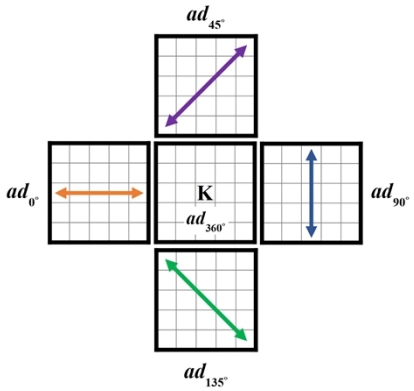

Fig. 5. The five angles considered by the variance criterion. All pixels ad_{360° in the sliding window and pixels ad_{0°, ad_{45°, ad_{90°, and ad_{135° in the four directions.

As mentioned above, the static region has a higher dispersion than the dynamic region, and with the increase of vessel depth, the dispersion of the dynamic region will increase due to tissue scattering, so selecting the minimum variance of the dynamic region will weaken this effect and enhance the imaging effect of deep vessels. When the MI is formed by three categories, the dynamic and static transition regions interact due to the dynamic and static scattering, so the median variance is selected to select a pixel set that is more representative of this region.

4. Results and discussion

4.1. Data and parameter selection

In this study, speckle images of in vitro phantoms at different depths and speckle image of rat cortical vessels were processed. Speckle image of rat cortical vessels are open-source data from GitHub [28]. In vitro phantom was used to simulate the vascular depth of $0\mu m$, $100\mu m$, $200\mu m$, $300\mu m$, $400\mu m$, $500\mu m$, using different epidermal depths. Thirty frames of OSIs were acquired

Biomedical Optics EXPRESS

at each depth with an image resolution of 1024×1024 pixels. The resolution of the rat cortical vessels image was 1280×1024 pixels.

For parameter selection, a parametric analysis was performed to determine the optimal parameter values. The CI used to generate the MI was generated using the sK method. The ADF used on the CI before cluster segmentation, the number of iterations n is 50, the diffusion rate λ=1/4, represents the four directions of similar pixels, and the edge amplitude coefficients were determined using the average contrast of the contrast images obtained in the previous iteration. Clustering takes k = 2, 3 into account for the analysis. The 2 classification will be divided into dynamic region and static region, and the 3 classification will be divided into dynamic region and transition region and static region, in which the region of interest is always dynamic region. Finally, combined with the classification results, k = 3 in the in vitro phantom processing and k = 2 in the rat cortical vessels speckle imaging. In the phantom experiment, the inner diameter of the capillary glass tube was 1 mm, the outer diameter was 2 mm, and the thickness was 0.5 mm. Because the inner diameter of the capillary glass tube was thicker than that of the capillary glass tube, and the absorption coefficient and scattering coefficient were different from those of the epidermal phantom (static region) and the fat emulsion of the simulated blood (dynamic region), the glass tube wall was divided into a separate category as the transient. Therefore, the in vitro data is divided into three categories. In vivo data are directly divided into two categories: tissues (static region) and blood vessels (dynamic region). In the application process, two or three classifications can be flexibly selected according to the difference between the thickness and the inner diameter of the tube. In vitro phantom experiments, considering the number of frames involved in the calculation of contrast value, the difference of CNR between three frames and thirty frames was not obvious after testing. In order to reduce the time required for imaging, all the vitro phantom experiments resulting images were calculated from three frames. The sliding window sizes for the asK, awK, sdK, and awsdK methods to calculate the contrast value are 3×3, 5×5, 9×9, 9×9, respectively. To avoid changing the flow velocity information, one frame of image was used for rat cortical vessels speckle contrast imaging, and sK was used instead of asK for comparison. The sliding window size of sK, awK, sdK and awsdK methods to calculate the contrast value is 9×9.

4.2. Validation and analysis of the awsdK

The first is to compare the CI obtained using different contrast methods at multiple depths (Fig. 6(a)). The effects of LSCI analysis methods can be distinguished by the degree of blood vessel visualization. The results show that the CI of awsdK method shows better visualization of vascular region, improves the contrast of dynamic and static regions and transition regions, and achieves greater noise attenuation. asK, awK and sdK can no longer clearly distinguish between dynamic and static regions at high depth, while awsdK can still show the difference between dynamic and static regions to realize the visualization of blood vessels. The value of CNR at the corresponding depth provides the results of CI visual analysis (Fig. 6(b)). awsdK is superior to the noise attenuation achieved by asK, awK and sdK, and achieves higher image quality improvement. With the increase of depth, compared with asK, the average CNR increases by 79.16%, 87.91%, 109.31%, 195.22%, 287.58% and 367.51%, respectively. Compared with sdK, the average CNR was increased by 26.74%, 32.85%, 51.72%, 110.42%, 177.39% and 163.80%, respectively. Compared with awK, the average CNR was increased by 55.89%, 51.31%, 57.38%, 137.20%, 216.31% and 239.29%, respectively. The adK method calculates the contrast value of the entire speckle image using the maximum variance direction criterion. As the depth of the glass tube increases, the dynamic region is increasingly affected by the static region, leading to greater fluctuations. Continuing to use the maximum variance direction criterion to calculate the contrast value has a small improvement on the CNR of the image. awK method uses adaptive window size to recalculate the contrast image for speckle image based on the segmented image,

Biomedical Optics EXPRESS

and this method has a small improvement on the overall CNR of the image. On the basis of awK method, the awsdK method adopts the maximum variance criterion to calculate the static region and the minimum method criterion to calculate the dynamic region, which can effectively reduce the influence of static speckle on dynamic speckle. As a result, awsdK can improve the visualization effect of blood vessels and has better imaging quality in deeper vascular imaging.

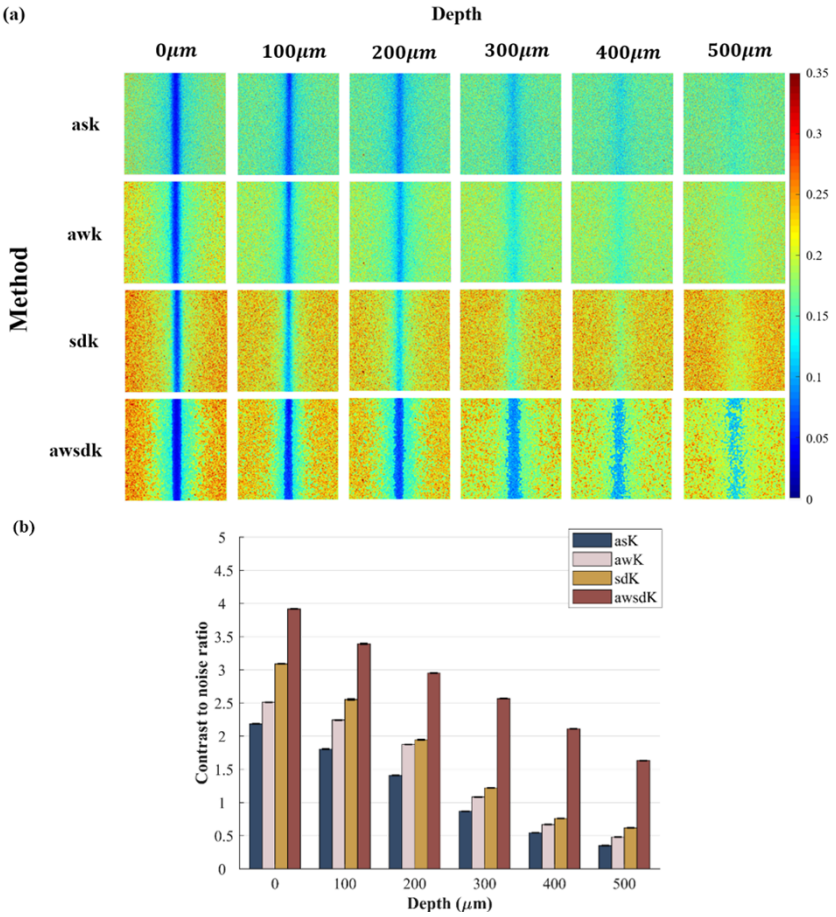

Fig. 6. a). Contrast images at different depths using different methods. b). CNR values corresponding to method and depth in (a).

Figure 7(a) is a comparison of CNR calculated by different imaging methods for the original speckle image at the same depth (depth=100μm) and different flow rates. By changing the blood flow velocity of the phantom, the blood flow velocity was taken as 5mm/s, 10mm/s, 15mm/s, and 20mm/s for comparison. The results show that at the same depth and different flow rates, awsdK can maintain higher CNR and obtain better quality images compared with asK, awK and sdK. Meanwhile, we used asK, awK, sdK and awsdK to measure $1/K^2$ at different flow velocities, where BFI = $1/K^2$, K represents the contrast value and BFI represents the relative blood flow velocity. After normalization for $1/K^2$, the relationship between the actual and relative flow velocities was plotted (Fig. 7(b)). It can be seen that the awsdK method is not much different from asK, awK, and sdK in terms of detecting traffic effectiveness, and these four methods also show that the relationship between $1/K^2$ and velocity is non-linear. Our proposed awsdK

Biomedical Optics EXPRESS

method improves the visualization of speckle contrast images without changing the flow velocity information.

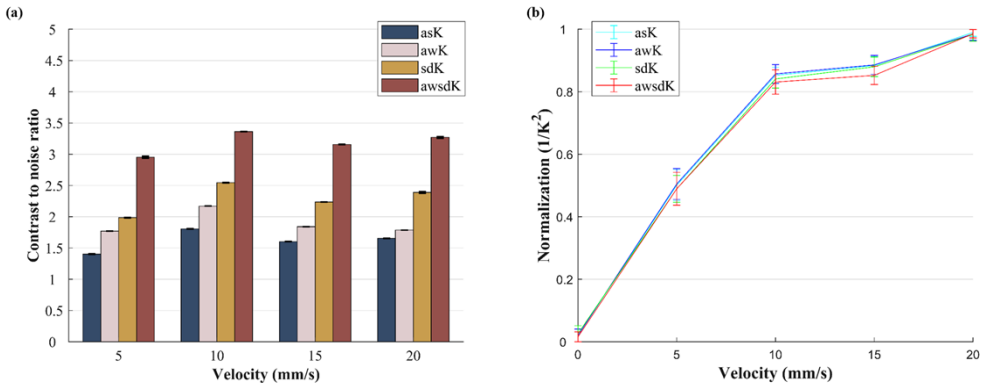

Fig. 7. a). CNR analysis of asK, awK, sdK, and awsdK at different velocity at a depth of 100μm. b). The relationship between the real flow velocity and relative velocity after processing with four contrast methods: asK, awK, sdK and awsdK.

4.3. *Rat cortical vessels speckle contrast imaging*

In addition, sK, awK, sdK and the proposed awsdK are tested in the OSI of rat cortical vessels with multiple vessel morphologies, in order to understand the performance of each method in the multi-vessel distribution. As can be seen from the results (Fig. 8), sK noise level is too high, the dynamic and static regions are not obvious, and the vascular information loss is serious. Although sdK increases the difference degree of dynamic and static regions, the direction with the largest variance is selected for global processing, which will reduce the visualization of small vessels with deep depth or small structure and slow flow speed, resulting in the loss of information of some small vessels. The CI obtained by awsdK method achieves noise attenuation and further enhances the contrast between static and dynamic regions, which can be reflected by the value of CNR. In addition, the small vascular structure is clearly distinguishable, and the vascular connectivity in the dynamic region is stronger, which increases the image extractable information. It should not be ignored that the proposed method can improve the vascular visualization while maintaining a high temporal resolution.

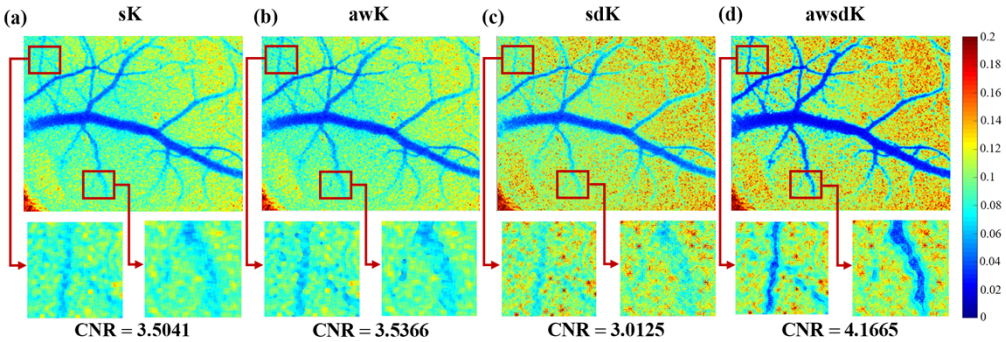

Fig. 8. Contrast images and corresponding CNR of rat cortical vessels using different methods. a). Using the sK method. b). Using the awK method. c). Using the sdK method. d). Using the awsdK method.

Biomedical Optics EXPRESS

Figure 9 shows the BFI maps of the rat cortical vessels speckle contrast images in different methods (BFI = $1/K^2$). BFI represents the relative blood flow velocity. Because the dynamic region is affected by the static speckle formed by static scattering, the contrast value of the dynamic region calculated by the traditional spatial contrast method will be higher, which may cause the loss of blood flow velocity information of deep vessels or small vessels. The awsdK method uses the adaptive window and the window direction criterion to recalculate the contrast image of OSI, which can reduce the noise in the dynamic region, improve the visualization of blood vessel flow velocity information, eliminate the influence of static scattering on deeper blood vessels or small blood vessels to the greatest extent, and show more blood flow velocity information of blood vessels.

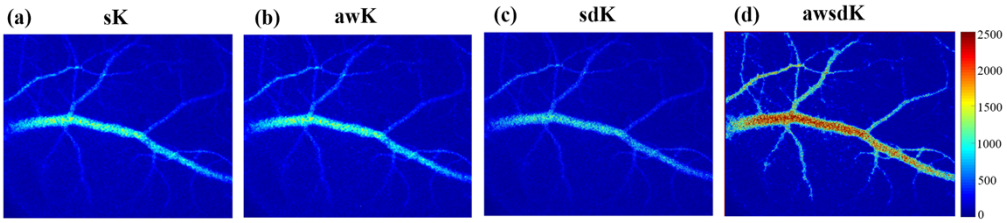

Fig. 9. The corresponding BFI maps of Fig. 8 a). Using the sK method. b). Using the awK method. c). Using the sdK method. d). Using the awsdK method.

5. Conclusion

In this study, we present a novel method, the awsdK method, which enables high noise attenuation while preserving high temporal resolution for contrast calculation in LSCI. Our approach utilizes different orientation standards for various regions of the image, resulting in improved contrast of dynamic and static regions, and provides better imaging quality with higher noise attenuation for deeper depths vascular imaging. Furthermore, to further enhance the contrast image of blood vessels, the pixels involved in contrast recalculation in the sliding analysis window were carefully screened in the boundary region, effectively removing inherent noise and improving the imaging effect of blood vessel edges and small blood vessels. The result is a clearer and more detailed contrast image of blood vessels. At the same time, we compared the imaging effects of asK (sK), awK, sdK and our proposed awsdK method in speckle images at different depths and speckle image of rat cortical vessels. CNR results show that sdK improves image quality, but the improvement is not as pronounced for deeper vascular imaging compared with awsdK. awK improved the visualization of blood vessel edges, but it does not significantly improve the overall imaging quality of the blood vessel compared to awsdK. In future work, the proposed method has the potential to be further improved for blood vessel segmentation and regional localization. We plan to validate our approach through in vivo experiments at deeper depths and in the presence of complex blood vessel distributions, as well as testing its ability to image different tissues.

Funding. National Natural Science Foundation of China (grant numbers 61905176); China Postdoctoral Science Foundation (No. 2019M651036); Natural Science Foundation of Tianjin City (No. 20JCQNJC00150); Tianjin Municipal Education Commission (No. 2019KJ022); Tianjin health and Health Committee Science and Technology Project (No. QN20015).

Disclosures. The authors declare that there are no conflicts of interest related to this article.

Data availability. Raw laser speckle images of rat cortical vessels are available on GitHub [28]. The other data underlying the results presented in this paper are not publicly available at this time but may be obtained from the authors upon reasonable request.

Biomedical Optics EXPRESS

References

1. C. Xu, F. W. Sellke, and M. R. Abid, "Assessments of microvascular function in organ systems," American Journal of Physiology-Heart and Circulatory Physiology **322**(6), H891–H905 (2022).
2. W. Feng, R. Shi, C. Zhang, S. J. Liu, T. T. Yu, and D. Zhu, "Visualization of skin microvascular dysfunction of type 1 diabetic mice using in vivo skin optical clearing method," J. Biomed. Opt. **24**(03), 1–9 (2018).
3. S. Y. Zhang, X. H. Yang, M. Jiang, L. H. Ma, J. Hu, and H. H. Zhang, "Post-transcriptional control by RNA-binding proteins in diabetes and its related complications," Front. Physiol. **13**, 953880 (2022).
4. L. Istvan, C. Czako, A. Elo, Z. Mihaly, P. Sotonyi, A. Varga, Z. Ungvari, A. Csiszar, A. Yabluchanskiy, S. Conley, T. Csipo, A. Lipecz, I. Kovacs, and Z. Z. Nagy, "Imaging retinal microvascular manifestations of carotid artery disease in older adults: from diagnosis of ocular complications to understanding microvascular contributions to cognitive impairment," Geroscience **43**(4), 1703–1723 (2021).
5. M. Wang, J. C. Hong, F. F. Zhou, and P. C. Li, "Application of laser speckle contrast imaging in the research on brain science," Prog. Biochem. Biophys. **48**, 922–937 (2021).
6. C. Qiu, J. Situ, S.-Y. Wang, and E. Vaghefi, "Inter-day repeatability assessment of human retinal blood flow using clinical laser speckle contrast imaging," Biomed. Opt. Express **13**(11), 6136–6152 (2022).
7. B. Lee, O. Sosnovtseva, C. M. Sørensen, and D. D. Postnov, "Multi-scale laser speckle contrast imaging of microcirculatory vasoreactivity," Biomed. Opt. Express **13**(4), 2312–2322 (2022).
8. S. Zheng and J. Mertz, "Direct characterization of tissue dynamics with laser speckle contrast imaging," Biomed. Opt. Express **13**(8), 4118–4133 (2022).
9. V. P. G. H. H. Anne, F. Edite, C. Carlos, and C. Joao, "Laser speckle imaging to monitor microvascular blood flow: a review," IEEE Rev. Biomed. Eng. **9**, 106–120 (2016).
10. C. Regan, C. Hayakawa, and B. Choi, "Momentum transfer Monte Carlo for the simulation of laser speckle imaging and its application in the skin," Biomed. Opt. Express **8**(12), 5708–5723 (2017).
11. J. Ramirez-San-Juan, C. Regan, B. Coyotl-Ocelotl, and B. Choi, "Spatial versus temporal laser speckle contrast analyses in the presence of static optical scatterers," J. Biomed. Opt. **19**(10), 106009 (2014).
12. F. Lopez-Tiro, H. Peregrina-Barreto, J. Rangel-Magdaleno, and J. C. Ramirez-San-Juan, "Visualization of in-vitro blood vessels in contrast images based on discrete wavelet transform decomposition," in *2019 IEEE International Instrumentation and Measurement Technology Conference (I2MTC)*, (2019), 1–6.
13. A. Rege, J. Senarathna, N. Li, and N. V. Thakor, "Anisotropic processing of laser speckle images improves spatiotemporal resolution," IEEE Trans. Biomed. Eng. **59**(5), 1272–1280 (2012).
14. C. E. Perez-Corona, H. Peregrina-Barreto, and J. C. Ramirez-San-Juan, "Space-directional approach to improve blood vessel visualization and temporal resolution in laser speckle contrast imaging," J. Biomed. Opt. **25**(03), 1–16 (2019).
15. C. E. Perez-Corona, H. Peregrina-Barreto, J. Rangel-Magdaleno, R. Ramos-Garcia, and J. C. Ramirez-San-Juan, "Space-directional laser speckle contrast imaging to improve blood vessels visualization," in *2018 IEEE International Instrumentation and Measurement Technology Conference (I2MTC)*, (2018), 1–5.
16. E. Morales-Vargas, H. Peregrina-Barreto, and J. C. Ramirez-San-Juan, "Adaptive processing for noise attenuation in laser speckle contrast imaging," Computer Methods and Programs in Biomedicine **212**, 106486 (2021).
17. J. Park, M. Ha, S. Yu, and B. Jung, "Fabrication of various optical tissue phantoms by the spin-coating method," J. Biomed. Opt. **21**(6), 065008 (2016).
18. D. Briers, D. D. Duncan, E. Hirst, S. J. Kirkpatrick, M. Larsson, W. Steenbergen, T. Stromberg, and O. B. Thompson, "Laser speckle contrast imaging: theoretical and practical limitations," J. Biomed. Opt. **18**(6), 066018 (2013).
19. J. D. Briers and W. Sian, "Laser speckle contrast analysis (LASCA): a nonscanning, full-field technique for monitoring capillary blood flow," J. Biomed. Opt. **1**(2), 174–179 (1996).
20. D. A. Boas and A. K. Dunn, "Laser speckle contrast imaging in biomedical optics," J. Biomed. Opt. **15**(1), 011109 (2010).
21. H. Y. Cheng, Q. M. Luo, S. Q. Zeng, S. B. Chen, J. Cen, and H. Gong, "Modified laser speckle imaging method with improved spatial resolution," J. Biomed. Opt. **8**(3), 559–564 (2003).
22. P. Perona and J. Malik, "Scale-space and edge detection using anisotropic diffusion," IEEE Trans. Pattern Anal. Machine Intell. **12**(7), 629–639 (1990).
23. L. P. Song, X. Y. Wang, R. Zhang, K. S. Zhang, Z. Zhou, and D. S. Elson, "Improving temporal resolution and speed sensitivity of laser speckle contrast analysis imaging based on noise reduction with an anisotropic diffusion filter," J. Opt. **20**(7), 075301 (2018).
24. X. Sang, B. Chen, D. Li, D. Q. Pan, and X. H. Sang, "Transient thermal response of blood vessels during laser irradiation monitored by laser speckle contrast imaging," Photonics **9**(8), 520 (2022).
25. K. P. Sinaga and M. S. Yang, "Unsupervised K-means clustering algorithm," IEEE Access **8**, 80716–80727 (2020).
26. A. K. Jain, "Data clustering: 50 years beyond K-means," Pattern Recognition Letters **31**(8), 651–666 (2010).
27. M. Welvaert and Y. Rosseel, "On the definition of signal-to-noise ratio and contrast-to-noise ratio for fMRI data," PLoS One **8**(11), e77089 (2013).
28. P. Keilbach, "pylsci," Github, 2023, https://github.com/pkeilbach/pylsci.